Applied Catalysis B: Environmental 232 (2018) 397–408

Contents lists available at ScienceDirect

Applied Catalysis B: Environmental

journal homepage: www.elsevier.com/locate/apcatb

N-Doped titanium dioxide nanosheets: Preparation, characterization and UV/visible-light activity

Zuzana Barbieriková[a], Eva Pližingrová[b,c,**], Monika Motlochová[b], Petr Bezdička[b], Jaroslav Boháček[b], Dana Dvoranová[a], Milan Mazúr[a], Jaroslav Kupčík[b], Jaromír Jirkovský[d], Jan Šubrt[b], Josef Krýsa[c], Vlasta Brezová[a,*]

[a] Institute of Physical Chemistry and Chemical Physics, Faculty of Chemical and Food Technology, Slovak University of Technology in Bratislava, Radlinského 9, SK-812 37 Bratislava, Slovak Republic
[b] The Czech Academy of Sciences, Institute of Inorganic Chemistry, Husinec-Řež č.p. 1001, CZ-250 68 Řež, Czech Republic
[c] Department of Inorganic Technology, University of Chemistry and Technology, Prague, Technická 5, CZ-166 28 Prague 6, Czech Republic
[d] The Czech Academy of Sciences, J. Heyrovský Institute of Physical Chemistry, Dolejškova 3, CZ-182 23 Prague, Czech Republic

ARTICLE INFO

Keywords:
N-Doped titanium dioxide
Photocatalysis
EPR spectroscopy
Lyophilization
Spin trapping

ABSTRACT

A series of nitrogen-doped 2D-titanium dioxide nanosheets was synthesized *via* green and facile procedure from the lyophilized aqueous colloids of peroxo titanic acid by urea addition and annealing in the temperature range of 350–500 °C. Detailed structural characterization (SEM, TEM with EDX, XRD) of N-doped TiO_2 confirmed their 2D-foil morphology composed of packed anatase nanocrystals. CHNS analysis showed that the total nitrogen content in the N-doped TiO_2 nanosheets is comparable (0.3 wt. %), and as shown in the EPR measurements in solid state, the annealing temperature determines the character of the nitrogen species incorporated in the anatase lattice. Paramagnetic nitrogen bulk centers ($N_b^{\bullet}$) dominate the X- and Q-band EPR spectra of the synthesized N-doped TiO_2 annealed up to 400 °C, while NO species were detected in samples annealed at higher temperatures. The photoexcitation of the N-doped anatase nanosheets resulted in an intense increase of the $N_b^{\bullet}$ signal intensity, especially upon VIS-light exposure, reflecting the selective photoexcitation of the material *via* diamagnetic N_b^- centers. Nevertheless, the situation upon irradiation of dispersed systems is rather different and to link the information on the structure of the nanosheets with their photoinduced performance in suspensions, the indirect techniques of EPR spectroscopy were applied. Effective generation of paramagnetic reactive oxygen species (ROS) upon UV photoexcitation of the N-doped TiO_2 nanopowders dispersed in water or dimethylsulfoxide was confirmed by EPR spin trapping technique. The VIS-light-induced ROS formation was significantly lower and correlates well with the results obtained by the photocatalytic decomposition of 4-chlorophenol upon VIS light. Even though the ·OH-induced capacity of N-doped TiO_2 prevails upon UV exposure, the VIS irradiation evokes the formation of photoelectrons capable of the selective reduction processes as demonstrated by the one-electron reduction of 2,2′-azinobis(3-ethylbenzothiazoline-6-sulfonate) radical cation, where the form of nitrogen dopant (e. g. the presence of $N_b^-/N_b^{\bullet}$) in the anatase structure showed a clear effect on the reaction rate. The prepared visible-light active N-doped TiO_2 nanosheets exhibiting also adequate UV photoactivity represent promising materials for further development of solar-light active photocatalysts.

1. Introduction

Major limitations of titanium dioxide in the context of its large-scale technological environmental application as photocatalyst come from its wide energy band gap, *i.e.* mainly UV light is necessary for the photoexcitation. Development of titania-based material which absorbs a substantial fraction of solar light represents the object of numerous studies, employing various approaches such as metal, non-metal doping, combination of photocatalysts, *etc.* [1–4]. Since the first reports on the visible (VIS) light activity of N-doped TiO_2 [5], a large part of these efforts has been directed towards this particular dopant [6–8]. As the improvement of the photocatalyst's performance goes hand in hand with the understanding of the primary processes of photoexcitation/activity, attention is focused on the electronic properties as well as the

* Corresponding author.
** Corresponding author at: The Czech Academy of Sciences, Institute of Inorganic Chemistry, Husinec-Řež č.p. 1001, CZ-250 68 Řež, Czech Republic.
E-mail addresses: plizingrova@iic.cas.cz (E. Pližingrová), vlasta.brezova@stuba.sk (V. Brezová).

https://doi.org/10.1016/j.apcatb.2018.03.053
Received 28 December 2017; Received in revised form 12 March 2018; Accepted 17 March 2018
Available online 19 March 2018
0926-3373/

charge carrier's dynamics of N-doped TiO_2 under irradiation [9–14]. The key points under debate on the optimal N-doped TiO_2 photocatalyst concern the quantity, chemical nature and the location in the solid of the N-species responsible for the VIS photoactivity to rationalize their specific role. In other words, the inert by-products of the chemical preparation, inevitably present in the solid, have to be distinguished from the species, which are playing an effective role in visible light absorption and molecular (photo)activation, which is crucial by choosing the most convenient preparation method [15–19]. The presence of two different nitrogen bulk species, *i.e.* substitutional N atoms (N_s) and interstitial nitrogen atoms bound to oxygen lattice ions (N_i), is coupled with the formation of localized N *2p* midgap energy states above the upper O *2p* valence band in anatase TiO_2 which are responsible for the alteration in the electronic band structure and the visible-light absorption [8–11,14]. The increased nitrogen doping level may result in the generation of both nitrogen bulk species, yet it can also lead to an enlarged fraction of surface nitrogen states acting as electron traps or recombination centers [19]. The implementation of nitrogen dopant in TiO_2 is significantly affected by the preparation method and an intensive research oriented on the synthetic pathways of N-doped TiO_2 photocatalysts, their structural and morphological characterization was performed in last decade [6,7,16,20]. The visible-light activity of synthesized photocatalysts is widely evaluated based on the photocatalytic degradation reactions of model compounds, in many cases various dyes, which can provide rather ambiguous results considering their VIS light absorption [21,22].

Herein we present a green and facile synthetic route for preparation of N-doped anatase nanomaterials with lamellar structure by an analogous approach as used in synthesis of highly active 2D-TiO_2 nanostructures [23,24]. The structural and electronic characterization of the newly prepared N-doped TiO_2 material was completed with the detailed EPR analysis to obtain insight into the character of the paramagnetic centers in the matrix of the anatase nanostructures reflecting the nitrogen doping in dark and under UV and VIS light irradiation of the solid-state samples. In the effort to link the information on the structure of the nanosheets with their photoinduced performance in dispersed systems, the indirect techniques of EPR spectroscopy were applied. The ability of N-doped TiO_2 photocatalysts to generate reactive oxygen species (ROS) upon *in situ* UV or VIS photoexcitation in water or dimethylsulfoxide suspensions was followed either using EPR spin trapping or by monitoring the one-electron reduction of 2,2′-azinobis(3-ethylbenzothiazoline-6-sulfonate) radical cation ($ABTS^{\cdot+}$) to the parent molecule ABTS. So obtained picture on the photoinduced electron transfer processes of N-doped TiO_2 photocatalysts in aqueous suspensions can be further compared with the effectiveness of the photocatalytic decomposition of 4-chlorophenol as a model compound.

2. Materials and methods

2.1. Chemicals

Titanium(IV) oxysulfate (titanyl sulfate, $TiOSO_4 \cdot x\,H_2O$, min. 29% Ti as TiO_2, Sigma-Aldrich) was used as a TiO_2 precursor. Urea ($CO(NH_2)_2$, ACS grade, Sigma-Aldrich) served as a nitrogen dopant source. During the preparation, aqueous solution of ammonia (NH_3, solution purum p.a., 25–29%, Penta) was used for precipitation of the precursor and hydrogen peroxide (H_2O_2, solution purum p.a., 30%, Penta) for pH reduction at the end of the synthesis. In the photocatalytic measurements 4-chlorophenol (4-CP, purity ≥ 99.9%, Sigma-Aldrich) was used as a model compound and titanium dioxide Aeroxide® P25 (Evonik) and Kronos VLP 7000 as the benchmarks.

The TiO_2 stock suspensions were prepared in distilled water or in dimethylsulfoxide (DMSO; SeccoSolv® Merck). The photoinduced generation of reactive radical intermediates was monitored by EPR spin trapping techniques using the 5,5-dimethyl-1-pyrroline *N*-oxide (DMPO, Sigma-Aldrich) distilled (70 Pa, 80–90 °C) prior to the application. 2,2′-Azinobis(3-ethylbenzothiazoline-6-sulfonic acid) diammonium salt (ABTS) and potassium persulfate ($K_2S_2O_8$) were obtained from Sigma-Aldrich and used as supplied. $K_2S_2O_8$ served as the oxidant in the oxidation of ABTS to the corresponding radical cation ($ABTS^{\cdot+}$) according to the previously reported procedure [25]. 4-Hydroxy-2,2,6,6-tetramethylpiperidine *N*-oxyl (Tempol, Sigma-Aldrich) was used as the calibration standard in EPR measurements.

2.2. Synthesis of N-doped samples

The synthesis of unmodified and modified titania nanoparticles was described in our previous papers [23,24,26]. At the beginning of the preparation, 4.80 g of titanyl sulfate were dissolved in 150 mL of distilled water at 35 °C. The transparent solution was cooled for about one hour in the freezer and afterwards the precipitation at approx. 0 °C by the aqueous ammonia was carried out, until the pH value reached 8. The white precipitate was filtered and washed several times to remove sulfate anions formed in the reaction. Filter cake was transferred into the beaker and re-suspended into 350 mL of distilled water. This white suspension was decanted and filtered two times. The pH value of the resulting suspension was reduced by adding 20 mL of hydrogen peroxide and the yellow suspension was stirred at laboratory temperature for approximately two hours until the solution turned from turbid yellow to transparent yellow. Thereafter urea was added into the yellow colloidal solution of peroxo titanic acid keeping the TiO_2 and urea in the ratios of 1:0.1, 1:0.5, or 1:1. So prepared colloidal solutions were dripped into liquid nitrogen and dried in the lyophilizator (10 mTorr, −56 °C). The lyophilized powders were annealed under air up to 350, 400, 450, 500 °C applying the heating rate of 1 °C min^{-1}; at the final temperatures the samples were held for 1 h.

The lyophilized doped samples are labeled as *TIG-N-urea portion-LYO*, *e.g., TIG-N-0.5-LYO* according to the different initial urea portion, the annealed samples are labeled as *TIG-N-urea portion-annealing temperature*, *e.g.*, *TIG-N-0.1-350*, and undoped samples as *TIG-annealing temperature*.

2.3. Characterization methods

Morphology and phase composition of the prepared samples were studied by methods of electron microscopy (SEM, HRTEM) and X-ray diffraction (XRD). CHNS analysis provided the information on the element composition and the fate of nitrogen present in the samples was followed by thermal analysis coupled with mass spectrometry measurements and by infrared (IR) spectroscopy. Electronic properties of the material were evaluated by XPS measurements and UV–VIS spectroscopy. Electron paramagnetic resonance (EPR) spectroscopy was applied to monitor the paramagnetic centers present in the powdered samples either in dark or upon photoexcitation using UV or visible light. The behavior of the N-doped anatase nanosheets upon irradiation was monitored also in suspension applying indirect techniques of EPR spectroscopy. To test the photocatalytic activity, the decomposition of 4-chlorophenol in the irradiated suspensions of prepared samples was investigated. All the technical details concerning the applied experimental techniques for characterization of prepared samples are provided in the Supplementary data.

3. Results and discussion

3.1. Characterization of N-doped 2D-titanium dioxide nanopowders

3.1.1. Morphological and phase characterization

According to our previous study [23,24], the applied method of preparation of distinctive TiO_2 nanostructures leads to the formation of nanosheet morphology, and modification of this process by adding metal dopant (Nd, Ag, Au) has no effect on the resulting morphology of the material [26]. Using SEM, analogous behavior was confirmed for all

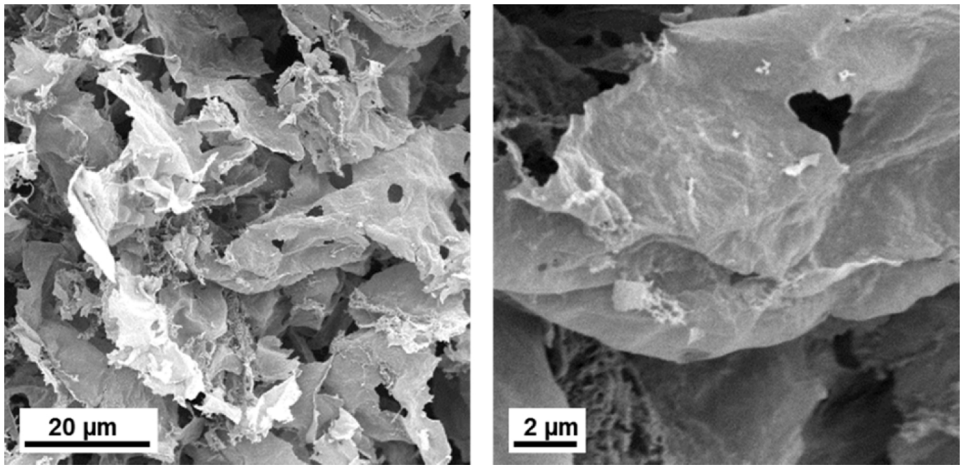

Fig. 1. SEM micrographs of *TIG-N-1-450*.

samples regardless on the TiO_2:urea ratio used in their synthesis and the porous layered structure was observed as shown for sample *TIG-N-1-450* in Fig. 1.

Nanosheets have a lateral size in the micron range (Fig. 2a), nevertheless their thickness is in the order of tens of nanometers, equally as we found previously for undoped 2D-TiO_2 samples [23,24] (*e.g.* AFM measurement confirmed thickness about 36 nm for sample *TIG-N-0.1-LYO*). According to the selected-area electron diffraction (SAED) pattern, given in Fig. 2b for the lyophilized (non-annealed) sample with the TiO_2:urea = 1:1 ratio, the nanosheets are comprised of amorphous peroxo titanic acid (Pdf 47-0124).

The annealed samples are made up of leaves consisting of anatase nanoparticles. Detailed morphology for the samples with the lowest and the highest urea portion annealed at 450 °C is shown in Fig. 3a and c, respectively. In the HRTEM mode the crystalline structure of these samples was observed (Fig. 3b,d). The EDX spectra were also recorded; however it is not possible to prove the presence of nitrogen in the sample due to the overlap of the nitrogen and titanium lines.

Unlike the previously prepared analogous TiO_2 nanosheets modified with Au, Ag, or Nd [26], which were annealed up to 950 °C exhibiting the presence of rutile phase for the highest temperatures, much lower annealing temperatures (350–500 °C) had to be applied for N-doped samples to preserve the presence of nitrogen dopant in the sample [9]. Consequently, the crystalline phase found corresponded to 100% of anatase in all samples (Table 1). No separate N-phase was observed in XRD measurements. The anatase crystalline phase was detected already at 350 °C in all samples, even though the diffraction lines were relatively broad and the intensity was quite low. The analogous trends in the XRD patterns reflecting the addition of urea, presented for samples annealed at 450 °C in Fig. 4 can be obtained for all the applied annealing temperatures. As discussed below, the thermal treatment of the lyophilized N-doped TiO_2 nanosheets in the temperature range of 350–500 °C resulted in the substantial decrease in nitrogen dopant content.

Table 1 summarizes the crystallite size and lattice parameters of synthesized N-doped anatase nanosheets, along with data obtained for pristine anatase 2D-nanostructures annealed at the identical temperatures. No significant differences in the values of anatase lattice parameters between N-doped and undoped samples were observed. N-doping at the lowest urea portion appears to reduce the size of the anatase crystals by almost one-third, whereas higher urea content applied in synthesis leads to a slight increase in the size of the anatase particles at annealing temperatures of 350–450 °C. At the annealing temperature of 500 °C, the size of the anatase crystals is comparable, therefore the influence of urea portion on the size of the anatase crystals has almost disappeared (Table 1).

The results of the surface area and porosity measurements are reported in Table 2. Depending on the shape of the adsorption/desorption curves (data not shown) and the pore size, it can be concluded that all samples are mesoporous. In the case of lyophilized samples higher urea content used in synthesis resulted in the lower surface area and the lower total pore volume. Only negligible effect of the annealing temperature on the total pore volume and average pore size was observed, with no trends revealed in N-doped samples. Contrary, in undoped

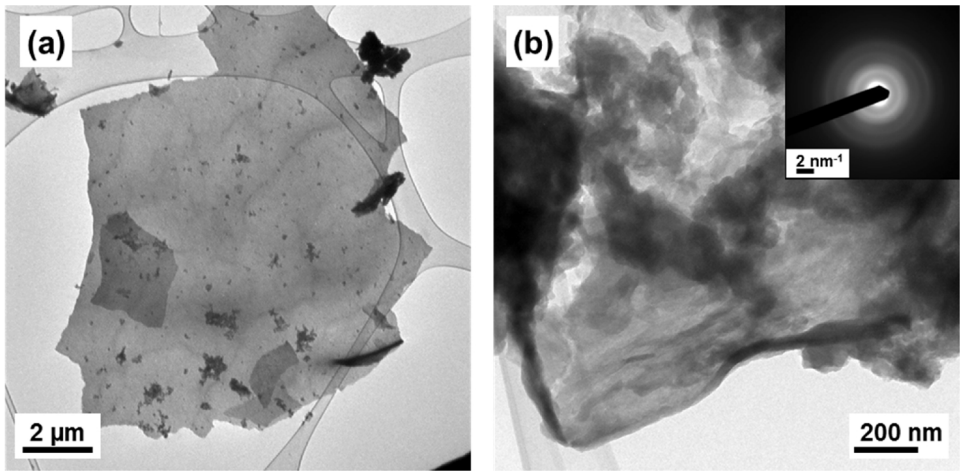

Fig. 2. (a) TEM micrograph of *TIG-N-0.1-LYO* and (b) TEM/ED micrograph of *TIG-N-1-LYO*.

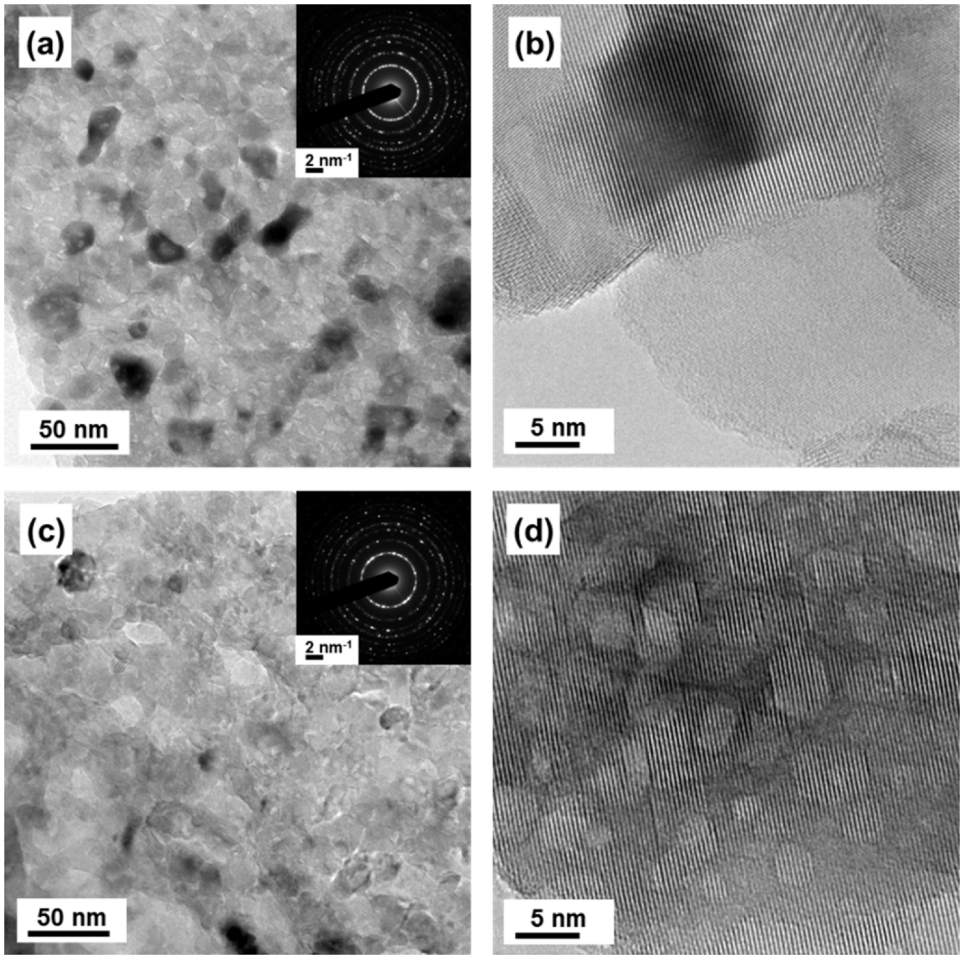

Fig. 3. TEM/ED and HRTEM micrographs of (a, b) *TIG-N-0.1-450* and (c, d) *TIG-N-1-450*.

samples the total pore volume significantly diminished upon annealing.

The results of CHNS measurements presented in Table 3 include all incinerable sulphur (< 0.1 wt. % in all samples, residuum of $TiOSO_4$ precursor) and incinerable carbon. Hydrogen content is affected by the moisture content in the samples. Firstly the content of nitrogen was assessed in the lyophilized samples, revealing 2.3 wt. % of nitrogen in the undoped sample *TIG-LYO* coming from ammonia used as a precipitating agent in the synthesis. The addition of urea during the synthesis correlates well with the increased nitrogen content detected for lyophilized samples *TIG-N-0.1-LYO, TIG-N-0.5-LYO* and *TIG-N-1-LYO* (Table 3). However, the temperature treatment of the lyophilized samples caused a significant decrease in the nitrogen content to 0.3 wt. % independent of the urea portion, as well as annealing temperature in the range of 350–500 °C. Consequently, we can conclude that for all annealed N-doped TiO_2 samples the total nitrogen content is comparable (0.3 wt. %), and the annealing temperature is expected to determine the character of the nitrogen species incorporated in the TiO_2 lattice.

To get a more detailed picture on the fate of nitrogen in the samples during annealing procedure, TA/MS analysis was performed (Fig. S1 in Supplementary data). Four reaction steps can be distinguished by the thermal decomposition of lyophilized N-doped samples, analogously as found for undoped peroxo titanates [27]. The first reaction step (30–100 °C) is characterized only by broad endothermic peak on DTA, connected with evaporation of humidity from the samples (m/z = 18). The second step is exothermic and according to MS, evolution of ammonia (m/z = 16 and 17) and nitrogen containing compounds (m/z = 14, 15, 28, 44, 45 and 46) begins. The third reaction step (200–450 °C) is also exothermic and not very well separated from the second step. Evolution of ammonia and nitrogen containing oxides continues and the mass spectra evidenced that the higher amount of urea is coupled with the higher and wider peaks of nitrogen containing compounds. While the transition of amorphous to crystalline phase is

Table 1
Phase composition and band gap values of the N-doped and undoped TiO_2 nanosheets annealed at different temperatures (350, 400, 450 and 500 °C).

Sample	Phase composition of anatase			Band gap (eV)	
	Crystallite size (nm)	Lattice parameters (Å)		E_{gi}	E_{ge}
		a	c		
TIG-N-0.1-350	13	3.7876	9.5061	3.2	2.4
TIG-N-0.1-400	16	3.7869	9.5083	3.2	2.5
TIG-N-0.1-450	16	3.7867	9.5111	3.2	2.6
TIG-N-0.1-500	17	3.7855	9.5107	3.3	–[a]
TIG-N-0.5-350	23	3.7880	9.5039	3.2	2.3
TIG-N-0.5-400	25	3.7877	9.5056	3.2	2.4
TIG-N-0.5-450	26	3.7864	9.5083	3.3	2.5
TIG-N-0.5-500	27	3.7861	9.5109	3.3	2.5
TIG-N-1-350	23	3.7880	9.5051	3.2	2.3
TIG-N-1-400	24	3.7874	9.5058	3.2	2.4
TIG-N-1-450	25	3.7865	9.5093	3.2	2.4
TIG-N-1-500	26	3.7857	9.5108	3.2	2.6
TIG-350	19	3.7876	9.5054	3.2	–
TIG-400	19	3.7868	9.5079	3.2	–
TIG-450	21	3.7867	9.5106	3.2	–
TIG-500	26	3.7860	9.5108	3.2	–

[a] The effect of N-doping on the diffuse reflectance spectrum was too low for determination of the corresponding band gap value (E_{ge}).

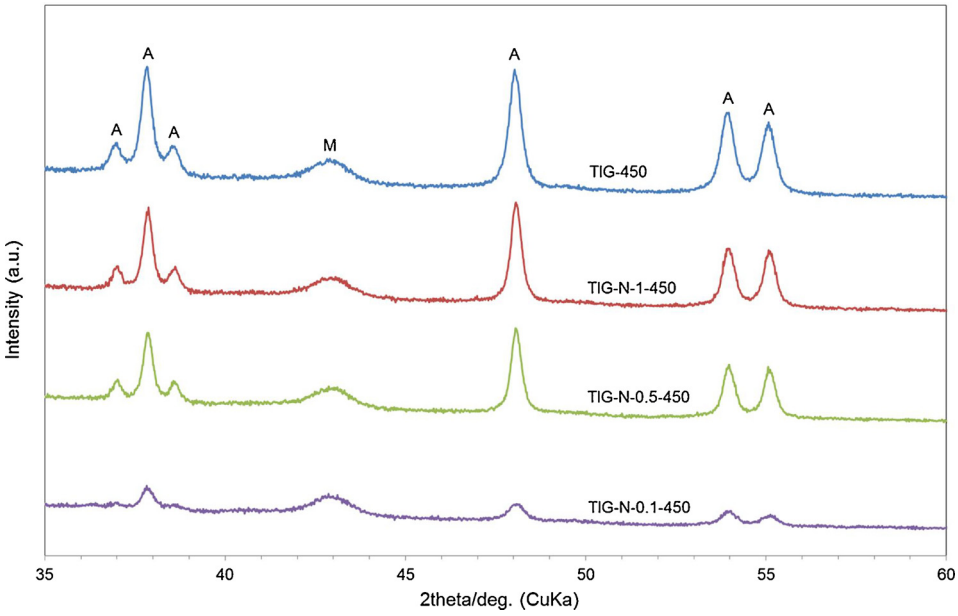

Fig. 4. XRD patterns of N-doped and undoped TiO_2 samples annealed at 450 °C (A – anatase, M – Mylar foil).

represented by a very sharp peak on DTA curve in the undoped samples [27], in the N-doped sample no crystallization peak is visible in the fourth decomposition step (450–1000 °C). The total mass loss for undoped samples is about 25%, the mass loss of N-doped sample is in range 30–60% dependent on the amount of urea used in synthesis (the higher urea portion the bigger the mass loss detected). Such behavior indicates a very slow crystallization of N-doped peroxo titanates and may correspond to only slight effect of annealing temperature (400–500 °C) on crystallite size detected by XRD (Table 1).

Infrared spectra also confirmed the destruction of urea upon annealing procedure as is shown for samples *TIG-N-1-LYO* and *TIG-N-1-500* in Fig. S2 in Supplementary data. While urea vibrations, *i.e.*, 3450 and 3340 cm^{-1}, $\nu(NH_2)$; 3260 cm^{-1}, comb(NH_2 + CO); 1680 cm^{-1}, $\delta(NH_2)$; 1600 cm^{-1}, ν(CO); 1466 cm^{-1}, ν(CN) [28]), along with the Ti-O-Ti vibration band in range of 400–600 cm^{-1} dominate the FTIR spectrum of *TIG-N-1-LYO*, upon annealing at 500 °C urea signals disappeared, which correlates well with the declared decrease in nitrogen content in *TIG-N-1-500* sample (Table 3). Further signals in *TIG-N-1-500* spectrum correspond to the vibration modes of anatase (500–900 cm^{-1}) with surface hydroxyl groups of adsorbed water [29].

Table 2
Summary of the results obtained by the surface area measurements of the lyophilized and annealed N-doped and undoped TiO_2 nanosheets.

Sample	Surface area ($m^2 g^{-1}$)	Total pore volume ($cm^3 g^{-1}$)	Average pore size (nm)
TIG-N-0.1-LYO	74	0.103	3.46
TIG-N-0.1-350	83	0.117	3.52
TIG-N-0.1-400	75	0.105	3.51
TIG-N-0.1-450	74	0.112	3.51
TIG-N-0.1-500	73	0.122	3.50
TIG-N-0.5-LYO	28	0.044	3.50
TIG-N-0.5-350	61	0.078	3.52
TIG-N-0.5-400	56	0.076	3.47
TIG-N-0.5-450	55	0.077	3.46
TIG-N-0.5-500	54	0.076	3.51
TIG-N-1-LYO	22	0.037	3.52
TIG-N-1-350	61	0.067	3.47
TIG-N-1-400	58	0.088	3.47
TIG-N-1-450	61	0.097	3.47
TIG-N-1-500	46	0.076	3.45
TIG- LYO	126	0.275	3.11
TIG-350	65	0.081	3.47
TIG-400	54	0.072	3.47
TIG-450	48	0.067	3.46
TIG-500	34	0.017	3.12

3.1.2. Electronic characterization

The chemical states of nitrogen in the synthesized N-doped anatase samples were examined using XPS analysis. According to the literature data N 1s signals with the binding energies in the range 396–397 eV are assigned to the substitutional nitrogen on oxygen sites in TiO_2 lattice, the peak ~400 eV was assigned to the interstitial N atoms [7,14,30], while peaks in the 398–401 eV are related to NO_x and NH_x species adsorbed on surface [7,15]. The survey scan spectrum measured in the range of 0–1000 eV binding energies for the lyophilized samples *TIG-N-0.1-LYO* and *TIG-N-1-LYO* demonstrates lines corresponding to titanium, carbon, nitrogen, and oxygen (Fig. 5a), identified as Ti 2p, N 1s, O 1s, and C 1s photoelectrons using the high resolution mode. The high resolution narrow spectra of N 1s for these lyophilized samples with peaks in the range of 398–401 eV reflect the presence of urea (Fig. 5b). However, after the thermal treatment in the temperature range of 350–500 °C, the signals of N 1s were not detected evidencing the removal of the adsorbed nitrogen species probably as gaseous NO or NO_2 [15]. This is in agreement with data obtained by TA/MS analysis (Fig. S1 in Supplementary data), as well as with the low nitrogen content confirmed in CHNS analysis (Table 3), which limited the application of

Table 3
Results of CHNS analysis of the lyophilized and annealed N-doped TiO_2 nanosheets.

Sample	Element content (wt. %)			
	N	C	H	S
TIG-N-0.1-LYO	5.9	2.6	2.5	0.03
TIG-N-0.1-350	0.3	0.6	0.5	0.03
TIG-N-0.1-500	0.3	0.2	0.3	0.03
TIG-N-0.5-LYO	17.0	7.0	3.6	0.02
TIG-N-0.5-350	0.3	0.2	0.4	0.04
TIG-N-0.5-500	0.3	–	0.2	0.04
TIG-N-1-LYO	26.2	11.0	4.6	0.08
TIG-N-1-350	0.3	0.3	0.5	0.08
TIG-N-1-500	0.3	0.2	0.2	0.08

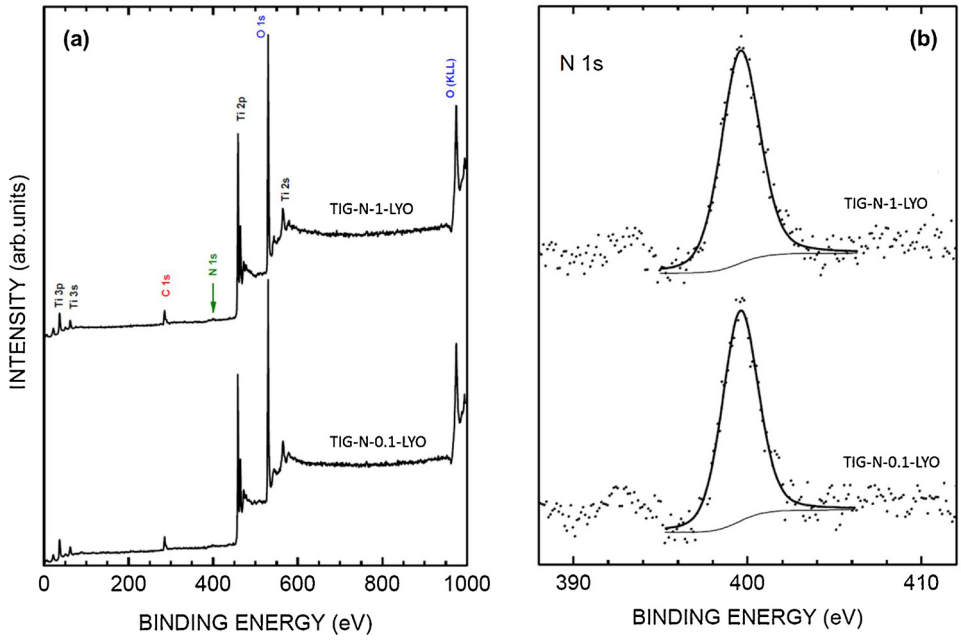

Fig. 5. XPS analysis: (a) survey scan spectrum of *TIG-N-0.1-LYO* and *TIG-N-1-LYO*; (b) spectrum for N 1s line of *TIG-N-0.1-LYO* and *TIG-N-1-LYO*.

XPS to follow the chemical states of nitrogen in the annealed samples [31].

The energy band gap of the N-doped samples was evaluated by Tauc plot analysis of diffuse reflectance (DR) spectra of the powdered samples. The DR spectra of *TIG-N-0.1* and *TIG-N-1* samples are given in Fig. 6. The increased absorption as a shoulder into the visible region is compatible with low nitrogen content in the annealed N-doped TiO_2 samples [32]. A double Boltzmann function was applied to determine the band gap values (Fig. S3 in Supplementary data). The calculated intrinsic and extrinsic band gap energies (E_{gi}, E_{ge}) for all N-doped samples are summarized in Table 1. While E_{gi} = 3.2 eV (388 nm) corresponds to the well-known value for anatase [33], the E_{ge} values in the range of 2.3–2.6 eV (539–477 nm) can be attributed to the N-dopant reflecting the transformation of chemical states of nitrogen caused by annealing as discussed below.

EPR spectroscopy is widely used to characterize doped/modified TiO_2 nanostructures, as in addition to the intrinsic paramagnetic centers, *e.g.*, Ti(III) species and oxygen vacancies coming from the synthesis or post-synthetic treatment [34–37], the paramagnetic centers containing the doping element can be identified [9,29,38–42]. Although different strategies have been used to incorporate nitrogen in titanium dioxide leading to slight changes in the material properties and chemical nature [18], the location of the species responsible for the photoactivity in visible light in the solid represents a crucial point [14,16,39,43–45]. Different chemical species like NO_x, substitutional N, or NH_x have been proposed as responsible of this effect [45]. Two types of paramagnetic species originating from nitrogen were previously identified in various N-doped TiO_2 nanostructured materials using EPR spectroscopy. Molecular nitrogen oxide species (NO) as products of complex oxidation processes of ammonium salts occurring upon calcination of the solid, may be trapped in microvoids of the porous solid [11,14]. More interesting paramagnetic species concerning the VIS activity frequently discussed in the N-doped TiO_2 represent the nitrogen centers, exhibiting a characteristic EPR signal with an orthorhombic *g*-tensor [9,14,38,46]. Based on the EPR spectra recorded previously under various conditions this specific signal was attributed to a monomeric nitrogen species incorporated in the bulk of N-doped TiO_2 ($N_b^{\bullet}$), as the species does not undergo dipolar broadening when oxygen is adsorbed at low temperature on the surface [11]. The $N_b^{\bullet}$ species is stable even at rather high temperature and is considered as the photoactive center responsible for the VIS activity of the material [9,11,47].

The X-band EPR spectra of all the studied N-doped anatase nanostructures measured in dark at 100 K revealed a significant effect of the annealing temperature on the character of the paramagnetic centers present in the TiO_2 matrix, as shown in Fig. 7 for the samples with the highest urea portion used in the synthesis. EPR spectra of the *TIG-N-1-350* and *TIG-N-1-400* exhibit the signal with characteristic *g*-tensor components g_1 = 2.005, g_2 = 2.004, g_3 = 2.003 and hyperfine couplings from the nitrogen A_1 = 0.23 mT, A_2 = 0.44 mT, A_3 = 3.23 mT, assigned to the nitrogen bulk species $N_b^{\bullet}$, with nitrogen atom bound to the lattice-oxygen ion [45]. Although this signal is observable also for the undoped sample *TIG-300*, as a result of the application of the aqueous ammonia in synthesis [26], but it is much more pronounced for the *TIG-N* samples reflecting the addition of urea. Increase of the annealing temperature above 400 °C led to a significant change in the spectrum. EPR signal with the spin Hamiltonian parameters g_1 = 2.001, g_2 = 1.998, g_3 = 1.927; A_1 < 0.1 mT, A_2 = 3.22 mT, A_3 = 0.96 mT dominates the spectrum of *TIG-N-1-450* and *TIG-N-1-500* (Fig. 7). This signal was previously detected in the EPR spectra of N-doped TiO_2 and corresponds to the nitric oxide, a by-product formed upon post-synthetic temperature treatment of the titania nanostructures containing nitrogen [47]. Unlike the nitrogen bulk species, NO does not influence the electronic structure of the solid *via* formation of midgap energy states [16,39].

While the intensity of the $N_b^{\bullet}$ signal stays relatively intact upon temperature increase up to 240 K with a rather well-resolved spectrum even at room temperature (Fig. 8a), the signal of NO decreases in the temperature range 100–240 K significantly (Fig. 8b). However, when the sample is cooled back to 100 K the signal is recovered. NO is thus expected to be present in closed pores within the crystalline structure and the corresponding EPR signal becomes visible when the molecule is weakly adsorbed and polarized on a cationic center at the inner surface of the cavity which occurs at low temperatures [16,43].

In addition to the paramagnetic centers originating from the introduction of nitrogen into the anatase matrix, EPR signal of axial symmetry with both parallel and perpendicular component below 2.000 was present in the EPR spectra of the samples annealed above 400 °C. The *g*-values obtained from the simulation of the experimental spectrum $g_{\perp}$ = 1.996, $g_{||}$ = 1.959 unambiguously point to the Ti(III)

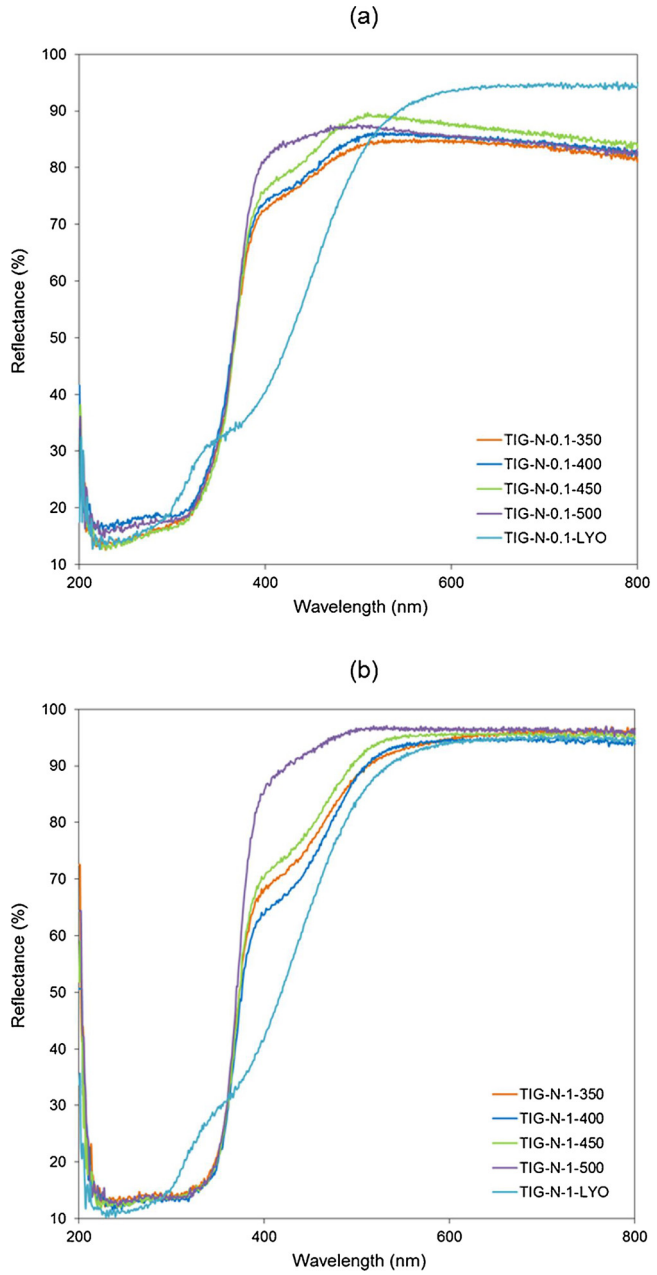

Fig. 6. UV–VIS DR spectra of (a) *TIG-N-0.1*, and (b) *TIG-N-1* lyophilized and annealed at different temperatures.

ions in a tetragonally distorted symmetry located in the anatase matrix [34].

Since in the EPR signal of $N_b^{\bullet}$ the orthorhombic *g*-tensor component values are very close [46], this species has been often investigated by a multifrequency approach, *i.e.* in addition to standard X-band measurements (9.5 GHz) higher frequency experiments in Q-band (35 GHz) were conducted [11]. Also in our study a higher sensitivity and better resolution of the EPR spectra of studied samples was expected in Q-band. As Fig. 7 shows, the spectra of N-doped TiO_2 reveal intense signals even at room temperature, unlike in the case of X-band experiments where low temperatures were necessary to obtain EPR spectra of satisfactory resolution and intensity. However the expected improvement in the resolution of the spectra measured at 100 K was not obtained. Also the effect of the annealing temperature on the character of individual spectra is less pronounced. Nevertheless, the Q-band EPR spectra obtained at 100 K reveal the signals of paramagnetic nitrogen species, either $N_b^{\bullet}$ or NO, depending on the annealing temperature, superimposed with a narrow signal characterized with axially symmetric *g*-tensor $g_{\perp} = 1.997$ and $g_{||} = 1.959$, well compatible with *g*-tensor of Ti(III) bulk centers in anatase lattice and a broad-line EPR signal at $g_{ef} \sim 2.00$ attributed to the hole-type centers [26]. Two higher field EPR signals with *g*-components in the region 1.973–1.968 are visible in the spectra of *TIG-N-1* especially for the samples annealed at higher temperatures. Similar signals were observed previously in the Q-band spectra of the analogous anatase nanosheets modified with metals [26]. Based on their characteristics and narrow line width it was proposed that they could reflect the generation of oxygen vacancies revealed as Ti(III) ions in specific local symmetries of anatase lattice [26,48,49]. The Q-band EPR spectra of the N-doped anatase nanosheets showed the presence of electron excess centers (Ti(III), oxygen vacancies [46,50]) in addition to the paramagnetic nitrogen centers well resolvable in the X-band.

3.2. Photoinduced activity of N-doped 2D-titanium dioxide nanopowders

3.2.1. Photoexcitation of TiO_2 powders at low temperatures (EPR)

The nitrogen bulk centers introduce localized electronic states in the titania gap either doubly occupied (diamagnetic N_b^-) or singly occupied (paramagnetic $N_b^{\bullet}$) independently of their specific lattice position (interstitial or substitutional) and the proper irradiation should promote electrons from these states to the conduction band [8,39,45,51]:

$$N_b^- \xrightarrow{h\nu} N_b^{\bullet} + e^- \quad (1)$$

$$N_b^{\bullet} \xrightarrow{h\nu} N_b^+ + e^- \quad (2)$$

In order to trace the photogenerated charge carriers as well as to follow the fate of the paramagnetic nitrogen species in the samples, the X-band EPR spectra of the *TIG-N* in dark and upon continuous *in situ* irradiation with either UV or VIS light at 100 K were monitored. Detection of directly observed single occupied paramagnetic species $N_b^{\bullet}$ implies the presence of doubly occupied diamagnetic N_b^- species in the anatase nanostructure as well, and both these species are affected by the visible-light irradiation [45]. As demonstrated in Fig. 9 in the case of *TIG-N-1-350* and *TIG-N-1-400* the photoexcitation (UV as well as VIS) caused an immediate growth of $N_b^{\bullet}$ signals. Considering the intense increase in the $N_b^{\bullet}$ signal intensity, explained by Eq. (1), diamagnetic N_b^- species are more abundant in the sample in correlation with the previous experimental and theoretical studies [46]. The response to visible light (160 klx) is significantly more intense compared to UV (λ_{max} = 365 nm; 20 mW cm^{-2}). Although the powdered samples were measured under air, no EPR signals of $O_2^{\bullet -}$ are present in the spectra. Even the prolonged exposure with the visible light up to 90 min did not exhibit the formation of surface superoxide radical anions [8,39,45]. Slight decrease of the $N_b^{\bullet}$ species signal could be explained by their interaction with light (Eq. (2)) or with Ti(III) centers [9,14], while the signal with $g < 2.000$ remains rather intact to the prolonged VIS exposure (Fig. S4 in Supplementary data). After switching of the LED source this decrease continues, however the repeated irradiation leads again to the increase of $N_b^{\bullet}$ signal.

The relatively intense spectrum of the nitric oxide can hinder the detection and identification of further species potentially formed upon photoexcitation of the anatase nanosheets, such as $O_2^{\bullet -}$ and Ti(III) ions [10]. The EPR signals of NO dominating the spectra of *TIG-N-1-450* and *TIG-N-1-500* are practically unchanged upon UV irradiation, however, in the case of *TIG-N-1-450* a signal of $N_b^{\bullet}$ appears, indicating the diamagnetic N_b^- centers are still present in the sample after annealing at 450 °C. Similar and even more pronounced effect can be seen upon VIS irradiation of *TIG-N-1-450*. Visible irradiation triggers the formation of detectable $N_b^{\bullet}$ EPR signal even for the sample *TIG-N-1-500*, although in this case the intensity of the NO signal decreases prominently. Analogous behavior was already observed and can be explained by the direct

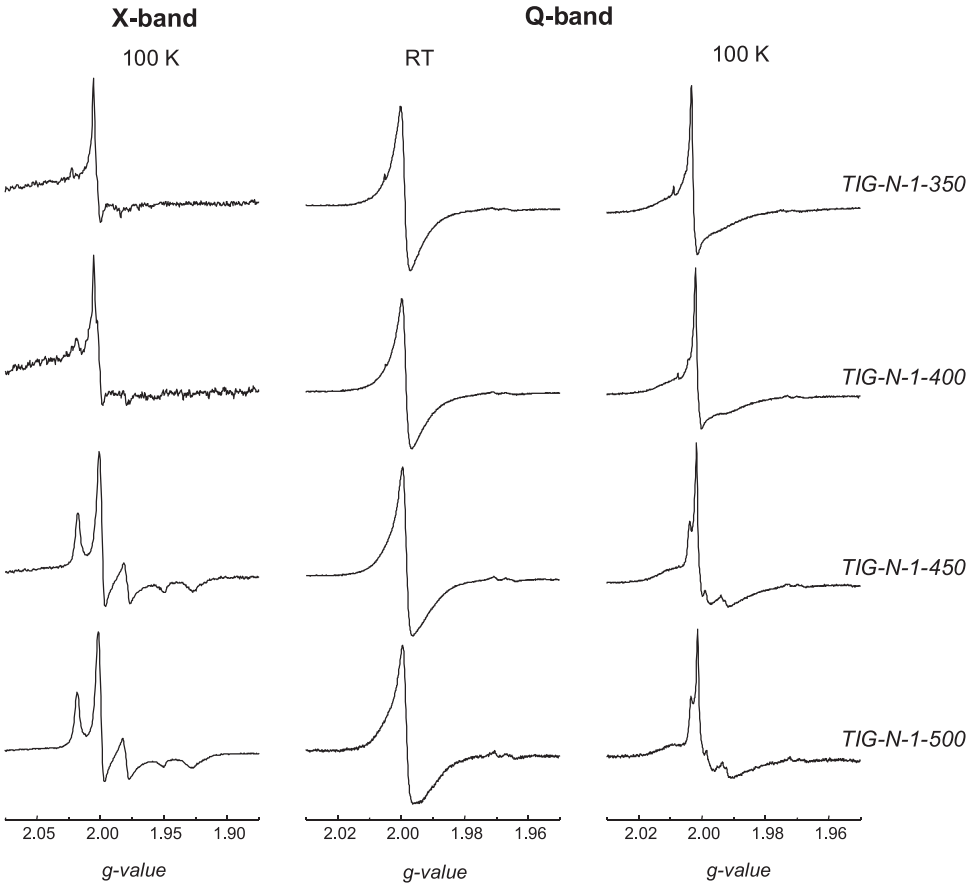

Fig. 7. X- and Q-band EPR spectra of *TIG-N-1* samples annealed at different temperatures measured in dark at 100 K and at RT.

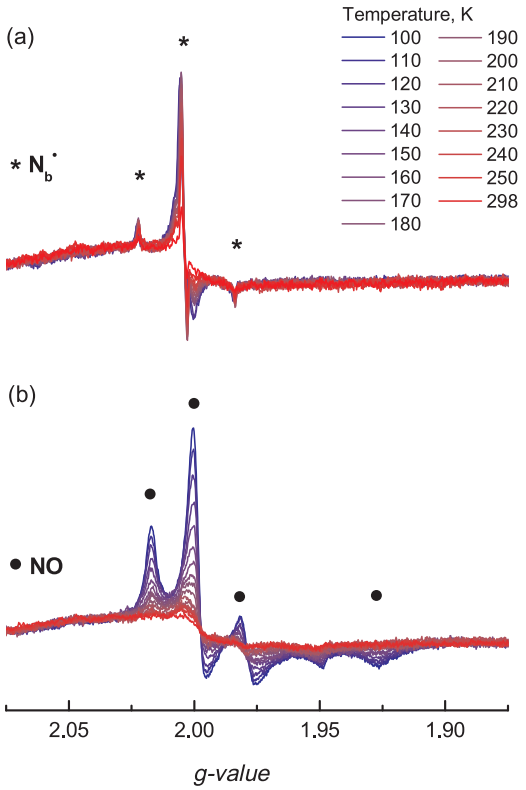

Fig. 8. X-band EPR spectra of (a) *TIG-N-1-350* and (b) *TIG-N-1-500* obtained upon increasing temperature in the range of 100–298 K.

interaction of the nitric oxide molecules with the visible light radiation [51], indicating different mechanisms of the N-doped anatase nanosheets photoexcitation upon UV and VIS irradiation.

3.2.2. *Photoexcitation of TiO_2 particulate systems (EPR spin trapping)*

EPR spin trapping technique, which enables the detection of transient radical intermediates, has been used to study photocatalytic systems containing TiO_2 for decades [52]. Standard spin trapping agent DMPO was applied to follow the generation of reactive oxygen species (ROS) upon photoexcitation of studied nanostructures in water or dimethyl sulfoxide (DMSO) suspensions under air.

Despite the intensive studies on N-doped TiO_2 photocatalysts, only limited information can be found in literature on reactive oxygen species generated upon VIS exposure [20,53,54]. To study the photogenerated ROS in water is an obvious choice of environment, due to the potential utilization of the material in water purification processes [52,55]. Spin-adduct ·DMPO-OH (spin Hamiltonian parameters; a_N = 1.499 mT, a_H^{β} = 1.485 mT; g = 2.0057) is commonly observed in the irradiated aerated TiO_2 aqueous suspensions containing DMPO spin trap [56]. The photoexcitation of aerated aqueous suspensions of all the studied N-doped nanopowders with either UV or VIS irradiation leads in both cases to the formation of ·DMPO-OH spin-adduct, as depicted in Fig. 10a for *TIG-N-1-350*. However, the intensity of the obtained signals differed significantly. In the case of UV photoexcitation rather intense signals of ·DMPO-OH were obtained, revealing the positive effect of the increasing annealing temperature, with the intensity for the *TIG-N-1-500* comparable to the one obtained for P25 under analogous conditions (data not shown). Upon VIS irradiation (even after prolonged exposure, 20 min) only very low-intensity signals were obtained without any trends revealed, concerning either the annealing temperature or mode of nitrogen doping. As the VIS photoexcitation does

Fig. 9. X-band EPR spectra obtained before and upon UV (λ_{max} = 365 nm; 20 mW cm^{-2}) or visible (160 klx) light photoexcitation of *TIG-N-1* samples annealed at different temperatures measured at 100 K.

not involve the formation of holes in the TiO_2 valence band [8,39,45,57], the generation of hydroxyl radicals could be explained by the alternative pathways including hydrogen peroxide produced by the disproportionation of $O_2\cdot^-$ in water [58,59].

The generation of $O_2\cdot^-$ is generally accepted in the UV photoexcited suspensions of anatase nanostructures [52]. Considering the low stability of $O_2\cdot^-$ and limited possibility to its detection by DMPO [60] in aqueous systems, aprotic dimethylsulfoxide was applied to monitor its formation upon photoexcitation of N-doped TiO_2 nanosheets. Immediately after the beginning of the UV photoexcitation of the system TiO_2/DMSO/DMPO/air, an EPR spectrum consisting of three individual signals was monitored. As expected, ·DMPO-O_2^- spin-adduct (a_N = 1.276 mT, a_H^β = 1.032 mT, a_H^γ = 0.139 mT; g = 2.0057; relative concentration 58%) dominated the spectrum. Further signals were attributed based on their Hamiltonian parameters to ·DMPO-OCH_3 spin-adduct (a_N = 1.311 mT, a_H^β = 0.803 mT, a_H^γ = 0.176 mT; g = 2.0057; 40%) and ·DMPO-CH_3 spin-adduct (a_N = 1.473 mT, a_H^β = 2.043 mT; g = 2.0056; 2%). These spin adducts formed by the addition of ·OCH_3 and ·CH_3 radicals to the DMPO are known to be present in analogous systems, due to the reaction of the DMSO solvent with the ROS [61]. The assignment of the individual spin-adducts was performed based on the simulation analysis presented in the Fig. S5 in the Supplementary data.

The visible-light activation of the powdered N-doped TiO_2 (annealed up to 450 °C) at 100 K under air resulted in a significant increase in the EPR signal intensity of $N_b^\bullet$ species which was expected to be coupled with the generation of surface $O_2\cdot^-$, however no EPR signals of superoxide radical anions were detected (Figs. 9 and S4 in Supplementary data). Nevertheless due to the intense response of *TIG-N-1-350* and *TIG-N-1-400* nanopowders to the VIS photoexcitation (Fig. 9), we anticipated this would translate into the increase in the concentration of ·DMPO-O_2^- spin-adduct monitored in the system TiO_2/DMSO/DMPO/air upon VIS irradiation. The VIS photoexcitation of the system led only to a low-intensity spectrum with dominant ·DMPO-O_2^- signal reflecting the selective photoexcitation of material *via* N_b^- (or $N_b^\bullet$) species present in the N-doped TiO_2 material (reaching 0.3 wt. % for samples annealed at 350 °C). A slight effect of the annealing temperature, which can be coupled with the presence of either N_b^- / $N_b^\bullet$ or NO, can be observed as *TIG-N-1-350* revealed the highest concentrations of ·DMPO-O_2^- which was about two times higher compared to the concentration obtained for P25 under analogous experimental conditions (data not shown).

3.2.3. *Photocatalytic reduction of paramagnetic ABTS·$^+$ to ABTS in water*

Another method to follow the redox processes in the irradiated TiO_2 suspensions is the one-electron reduction of a semi-stable radical cation ABTS·$^+$ [42,62], based on the monitoring of its over-modulated EPR spectrum (g = 2.0036, [42]). Changes in the intensity of this signal upon irradiation can be linked to the effect of the photocatalyst, since the blank experiments upon both UV and VIS irradiation, proved sufficient photostability of ABTS·$^+$ under the given experimental conditions. The decrease in ABTS·$^+$ concentration in the aqueous suspensions containing the synthesized anatase nanopowders or P25 as the benchmark was followed *in situ* either during a 100-s UV exposure (λ_{max} = 365 nm, 19 mW cm^{-2}) or during a 600-s VIS exposure (160 klx) (Fig. 11). In the irradiated aqueous TiO_2 suspensions radical cation

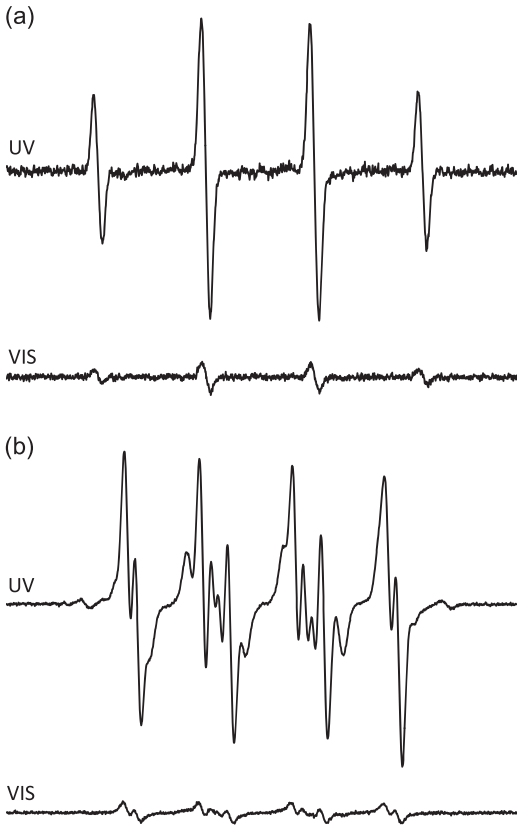

Fig. 10. The EPR spectra (magnetic field sweep width, $SW = 7$ mT) obtained upon UV or VIS photoexcitation of the aerated (a) water or (b) DMSO suspensions of *TIG-N-1-350* containing DMPO spin trapping agent. Initial concentrations: $c(TiO_2) = 0.33\ g\ L^{-1}$; $c_0(DMPO) = 0.03$ M.

ABTS$^{\bullet+}$ is reduced to ABTS *via* photoelectrons and *via* superoxide radical anions [42,62,63], generated instantly by the reaction of the photoelectrons with the molecular oxygen. The inset in Fig. 11a shows how the concentration of ABTS$^{\bullet+}$ is diminished in the presence of *TIG-N-1-350* and the pristine *TIG-800* upon UV irradiation reaching the zero value in 100 or 60 s, respectively. Upon continuous UV irradiation the formal first-order rate constants of ABTS$^{\bullet+}$ reduction calculated for the series of N-doped samples and undoped nanostructures annealed at temperatures 300, 500 and 800 °C revealed the most pronounced effect for the undoped *TIG-800* comparable with the benchmark P25. Obviously the effectiveness of this process is positively affected mainly by the presence of well-defined anatase nanocrystals in the material due to sufficiently high annealing temperature. All the samples annealed at temperatures below 500 °C, N-doped as well as undoped, exhibit a rather comparable results of about half the value in the case of *TIG-800* and P25. The activity of the nanostructures upon UV irradiation is coupled with the presence of a sufficient amount of anatase nanocrystals, reflecting the standard mechanism of TiO_2 photoexcitation, *i.e.* effective formation of charge carriers and their further reactions with molecules present in the system. On the other hand, visible light does not provide enough energy to induce this process which reflects no effect of *TIG-800* and P25 on the ABTS$^{\bullet+}$ concentration upon continuous VIS irradiation. Here, however the reduction of the radical cation was observed by the samples containing bulk nitrogen species $N_b^-/N_b^\bullet$ in the matrix. As was proved previously [26], also the undoped samples contained nitrogen, due to the application of ammonia during synthesis, which explains the comparable rate constants obtained for *TIG-N-1-350* and *TIG-300*, and for *TIG-N-1-500* and *TIG-500*. Effect of the annealing temperature is significant, as shows Fig. 11b, reflecting the amount of nitrogen present in the TiO_2 structure in the form of $N_b^-/N_b^\bullet$ species and we can propose that ABTS$^{\bullet+}$ is reduced *via*

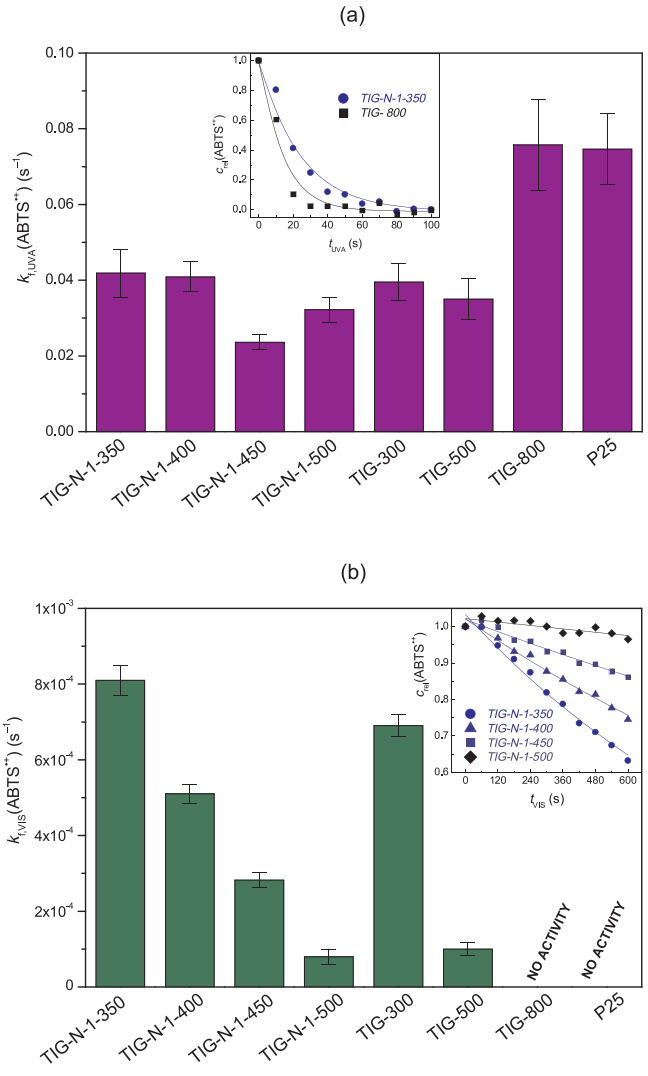

Fig. 11. Formal rate constants of ABTS $^{\bullet+}$ reduction in the presence of studied TiO_2 nanostructures (and P25) in water upon continuous (a) UV ($\lambda_{max} = 365$ nm; 19 mW cm^{-2}) or (b) VIS (160 klx) irradiation evaluated from the EPR spectra. Initial concentrations: $c(TiO_2) = 0.33\ g\ L^{-1}$; c_0 (ABTS$^{\bullet+}$) = 56 μM. Inset: Dependence of the ABTS$^{\bullet+}$ relative concentration on the irradiation time measured under analogous conditions.

photogenerated electrons coming from the selective VIS excitation of $N_b^\bullet/N_b^-$ (Eqs. (1) and (2)).

3.2.4. Photocatalytic decomposition of 4-CP

The photocatalytic performance of the prepared N-doped TiO_2 samples was monitored following the decomposition of 4-CP upon UV (Inset in Fig. 12a) or upon VIS (Fig. 12b) irradiation. The formal first-order rate constants for N-doped samples with the lowest and the highest urea portion *TIG-N-0.1*, *TIG-N-1* along with undoped analogs annealed at 400 and 500 °C and P25 are given in Fig. 12a. Much lower photocatalytic ability of annealed samples *TIG-N-1* than *TIG-N-0.1* can be attributed to the differences in surface area (Table 2) affecting the efficient adsorption of 4-CP. The oxidation processes involved in the photocatalytic decomposition of the model compound 4-CP are coupled with the effective generation of photogenerated holes and hydroxyl radicals in the aqueous TiO_2 suspensions and these processes are influenced by the presence of N-dopant. Despite the nitrogen content determined by CHNS analysis for the synthesized N-doped is comparable (Table 3), our EPR experiments confirmed significant effect of annealing temperature on the chemical states of nitrogen which could

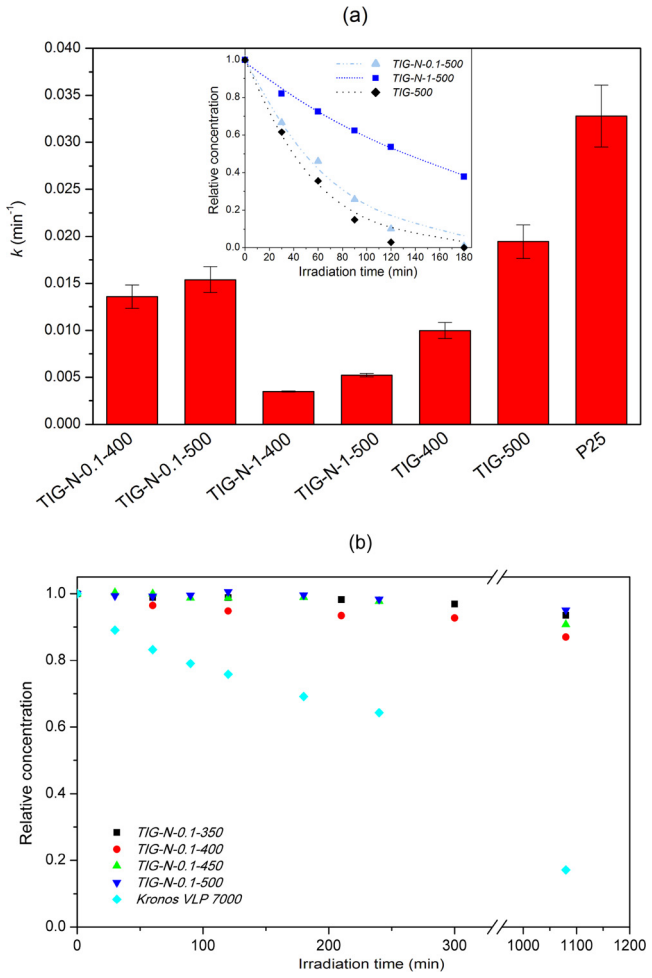

Fig. 12. (a) Formal rate constants of 4-CP decomposition upon UV irradiation in the presence of studied TiO_2 nanostructures and P25. Inset: UV-induced photocatalytic decomposition of 4-CP in the aerated aqueous suspensions of *TIG-N-0.1*, *TIG-N-1*, and undoped samples annealed at 500 °C. (b) Photocatalytic decomposition of 4-CP in the aerated aqueous suspensions of *TIG-N-0.1* annealed at 350–500 °C and Kronos VLP 7000 upon visible-light irradiation. Initial concentrations: $c(TiO_2) = 0.15\,g\,L^{-1}$, $c_0(4\text{-CP}) = 5 \times 10^{-5}\,M$.

affect the reactions on surface upon UV exposure.

The 4-CP decomposition upon VIS photoexcitation of the studied samples was very low, as even the most active *TIG-N-0.1-400* sample did not provide results comparable to the standard Kronos VLP 7000 (Fig. 12b) in good correlation with the limited generation of hydroxyl radical DMPO spin-adduct found by EPR spin trapping technique (Fig. 10).

4. Conclusions

A green and facile synthetic method was applied to prepare a series of nitrogen-doped 2D-titanium dioxide nanosheets from the lyophilized aqueous colloids of peroxo titanic acid by urea addition and annealing in the temperature range of 350–500 °C. Detailed structural characterization (SEM, TEM with EDX, XRD) of N-doped TiO_2 confirmed their 2D-foil morphology composed of packed anatase nanocrystals. The N-doping led to the formation of paramagnetic nitrogen bulk centers ($N_b^{\bullet}$) and/or NO species in the anatase lattice detected by X- and Q-band spectroscopy. The X-band EPR spectra measured at 100 K upon *in situ* UV or VIS photoexcitation evidenced the role of $N_b^{\bullet}$ centers in the visible light response of N-doped anatase nanosheets, monitoring the intense increase in the $N_b^{\bullet}$ signal intensity especially upon VIS-light exposure. Upon UV photoexcitation the N-doped TiO_2 nanopowders dispersed in water or DMSO effectively generate ROS (hydroxyl radical, superoxide radical anion) detected as the corresponding DMPO spin-adducts. The VIS-light-induced ROS formation was significantly lower and correlates well with the photoactivity followed by the photocatalytic decomposition of 4-chlorophenol. While the UV photoexcitation of N-doped TiO_2 nanosheets dispersed in water led to the efficient generation of hydroxyl radicals following the reaction pathways including photogenerated holes and electrons in the presence of oxygen [52], the visible-light photoactivation pathway involves the N_b^- excitation generating $N_b^{\bullet}$ species and photoelectrons as the key player in the ROS production. Even so the ·OH-induced capacity of N-doped TiO_2 prevails upon UV exposure, the VIS irradiation evokes the reduction reactions of photoelectrons, which may be employed in the selective reduction processes. This was demonstrated by the one-electron reduction of 2,2′-azinobis(3-ethylbenzothiazoline-6-sulfonate) radical cation showing a clear effect of the form of nitrogen dopant in the anatase structure on the reaction rate, as the highest values were obtained for the samples containing $N_b^-/N_b^{\bullet}$ annealed at lowest temperatures. The results point to a significant impact of the chemical states in which nitrogen is present in the structure on the reactions on surface of N-doped anatase nanosheets upon exposure. The prepared visible-light active N-doped TiO_2 nanosheets exhibiting also adequate UV photoactivity represent promising materials for further development of solar-light active photocatalysts.

Acknowledgements

This study was financially supported by the Ministry of Education, Youth and Sports of the Czech Republic (Research Infrastructure NanoEnviCz, No. LM2015073 and project INTER EXCELLENCE, No. LTACH17007), Multilateral Scientific and Technological Cooperation in the Danube Region (MSMT 8X17016), Scientific Grant Agency of the Slovak Republic (VEGA Project 1/0026/18) and the Slovak Research and Development Agency under the contract No. DS-2016-0016. The authors gratefully acknowledge Ivana Darvasiová and Lukáš Gál for technical assistance, Lenka Volfová for the UV–VIS measurements, and Zdeněk Bastl for XPS measurements.

Appendix A. Supplementary data

Supplementary material related to this article can be found, in the online version, at doi:https://doi.org/10.1016/j.apcatb.2018.03.053.

References

[1] S.G. Kumar, K.S.R.K. Rao, Comparison of modification strategies towards enhanced charge carrier separation and photocatalytic degradation activity of metal oxide semiconductors (TiO_2, WO_3 and ZnO), Appl. Surf. Sci. 391 (2017) 124–148.
[2] B. Liu, Y. Fang, Z. Li, S. Xu, Visible-light nanostructured photocatalysts – a review, J. Nanosci. Nanotechnol. 15 (2015) 889–920.
[3] S. Dong, J. Feng, M. Fan, Y. Pi, L. Hu, X. Han, M. Liu, J. Sun, Recent developments in heterogeneous photocatalytic water treatment using visible light-responsive photocatalysts: a review, RSC Adv. 5 (2015) 14610–14630.
[4] M. Pelaez, N. Nolan, S. Pillai, M. Seery, P. Falaras, A. Kontos, P. Dunlop, J. Hamilton, J. Byrne, K. O'Shea, M. Entezari, D. Dionysiou, A review on the visible light active titanium dioxide photocatalysts for environmental applications, Appl. Catal. B 125 (2012) 331–349.
[5] R. Asahi, T. Morikawa, T. Ohwaki, K. Aoki, Y. Taga, Visible-light photocatalysis in nitrogen-doped titanium oxides, Science 293 (2001) 269–271.
[6] R. Asahi, T. Morikawa, H. Irie, T. Ohwaki, Nitrogen-doped titanium dioxide as visible-light-sensitive photocatalyst: designs, developments, and prospects, Chem. Rev. 114 (2014) 9824–9852.
[7] A.V. Emeline, V.N. Kuznetsov, V.K. Rybchuk, N. Serpone, Visible-light-active titania photocatalysts: the case of N-doped TiO_2s-properties and some fundamental issues, Int. J. Photoenergy 2008 (2008) ID 258394.
[8] M. D'Arienzo, N. Siedl, A. Sternig, R. Scotti, F. Morazzoni, J. Bernardi, O. Diwald, Solar light and dopant-induced recombination effects: photoactive nitrogen in TiO_2 as a case study, J. Phys. Chem. C 114 (2010) 18067–18072.
[9] M. D'Arienzo, R. Scotti, L. Wahba, C. Battocchio, E. Bemporad, A. Nale, F. Morazzoni, Hydrothermal N-doped TiO_2: explaining photocatalytic properties by electronic and magnetic identification of N active sites, Appl. Catal. B 93 (2009) 149–155.
[10] G. Barolo, S. Livraghi, M. Chiesa, M.C. Paganini, E. Giamello, Mechanism of the

photoactivity under visible light of N-doped titanium dioxide. Charge carriers migration in irradiated N-TiO_2 investigated by electron paramagnetic resonance, J. Phys. Chem. C 116 (2012) 20887–20894.
[11] C. Di Valentin, E. Finazzi, G. Pacchioni, A. Selloni, S. Livraghi, M.C. Paganini, E. Giamello, N-doped TiO_2: theory and experiment, Chem. Phys. 339 (2007) 44–56.
[12] C. Di Valentin, G. Pacchioni, A. Selloni, Origin of the different photoactivity of N-doped anatase and rutile TiO_2, Phys. Rev. B: Condens. Matter Mater. Phys. 70 (2004) 085116-085111–085116-085114.
[13] K.I. Yamanaka, T. Morikawa, Charge-carrier dynamics in nitrogen-doped TiO_2 powder studied by femtosecond time-resolved diffuse reflectance spectroscopy, J. Phys. Chem. C 116 (2012) 1286–1292.
[14] F. Napoli, M. Chiesa, S. Livraghi, E. Giamello, S. Agnoli, G. Granozzi, G. Pacchioni, C. Di Valentin, The nitrogen photoactive centre in N-doped titanium dioxide formed via interaction of N atoms with the solid. Nature and energy level of the species, Chem. Phys. Lett. 477 (2009) 135–138.
[15] K.A. Borges, L.M. Santos, R.M. Paniago, N.M. Barbosa Neto, J. Schneider, D.W. Bahnemann, A.O.T. Patrocinio, A.E.H. Machado, Characterization of a highly efficient N-doped TiO_2 photocatalyst prepared: via factorial design, New J. Chem. 40 (2016) 7846–7855.
[16] S. Livraghi, M. Pelaez, J. Biedrzycki, I. Corazzari, E. Giamello, D.D. Dionysiou, Influence of the chemical synthesis on the physicochemical properties of N-TiO_2 nanoparticles, Catal. Today 209 (2013) 54–59.
[17] H.M. Yates, M.G. Nolan, D.W. Sheel, M.E. Pemble, The role of nitrogen doping on the development of visible light-induced photocatalytic activity in thin TiO_2 films grown on glass by chemical vapour deposition, J. Photochem. Photobiol. A 179 (2006) 213–223.
[18] S.A. Ansari, M.M. Khan, M.O. Ansari, M.H. Cho, Nitrogen-doped titanium dioxide (N-doped TiO_2) for visible light photocatalysis, New J. Chem. 40 (2016) 3000–3009.
[19] J. Wang, K. Tapio, A. Habert, S. Sorgues, C. Colbeau-Justin, B. Ratier, M. Scarisoreanu, J. Toppari, N. Herlin-Boime, J. Bouclé, Influence of nitrogen doping on device operation for TiO_2-based solid-state dye-sensitized solar cells: photo-physics from materials to devices, Nanomaterials 6 (2016) 35.
[20] F. Wang, X. He, L. Sun, J. Chen, X. Wang, J. Xu, X. Han, Engineering an N-doped TiO_2@N-doped C butterfly-like nanostructure with long-lived photo-generated carriers for efficient photocatalytic selective amine oxidation, J. Mater. Chem. A 6 (2018) 2091–2099.
[21] N. Barbero, D. Vione, Why dyes should not be used to test the photocatalytic activity of semiconductor oxides, Environ. Sci. Technol. 50 (2016) 2130–2131.
[22] M. Rochkind, S. Pasternak, Y. Paz, Using dyes for evaluating photocatalytic properties: a critical review, Molecules 20 (2015) 88–110.
[23] J. Šubrt, P. Pulišová, J. Boháček, P. Bezdička, E. Pližingrová, L. Volfová, J. Kupčík, Highly photoactive 2D titanium dioxide nanostructures prepared from lyophilized aqueous colloids of peroxo-polytitanic acid, Mater. Res. Bull. 49 (2014) 405–412.
[24] E. Pližingrová, L. Volfová, P. Svora, N.K. Labhsetwar, M. Klementová, L. Szatmáry, J. Šubrt, Highly photoactive anatase foams prepared from lyophilized aqueous colloids of peroxo-polytitanic acid, Catal. Today 240 (2015) 107–113.
[25] R. Re, N. Pellegrini, A. Proteggente, A. Pannala, M. Yang, C. Rice-Evans, Antioxidant activity applying an improved ABTS radical cation decolorization assay, Free Radic. Biol. Med. 26 (1999) 1231–1237.
[26] E. Pližingrová, M. Klementová, P. Bezdička, J. Boháček, Z. Barbieriková, D. Dvoranová, M. Mazúr, J. Krýsa, J. Šubrt, V. Brezová, 2D-Titanium dioxide nanosheets modified with Nd, Ag and Au: preparation, characterization and photocatalytic activity, Catal. Today 281 (2017) 165–180.
[27] M. Palkovská, V. Slovák, J. Šubrt, J. Boháček, J. Havlín, Thermal decomposition of a peroxopolytitanic acid cryogel: TA/MS study, Thermochim. Acta 647 (2017) 1–7.
[28] R. Keuleers, H.O. Desseyn, B. Rousseau, C. Van Alsenoy, Vibrational analysis of urea, J. Phys. Chem. A 103 (1999) 4621–4630.
[29] D. Dvoranová, V. Brezová, M. Mazúr, M.A. Malati, Investigations of metal-doped titanium dioxide photocatalysts, Appl. Catal. B 37 (2002) 91–105.
[30] R. Quesada-Cabrera, C. Sotelo-Vázquez, M. Quesada-González, E.P. Melián, N. Chadwick, I.P. Parkin, On the apparent visible-light and enhanced UV-light photocatalytic activity of nitrogen-doped TiO_2 thin films, J. Photochem. Photobiol. A 333 (2017) 49–55.
[31] M. Palkovská, V. Slovák, J. Šubrt, J. Boháček, Z. Barbieriková, V. Brezová, R. Fajgar, Investigation of the thermal decomposition of a new titanium dioxide material: TA/MS and EPR study, J. Therm. Anal. Calorim. 125 (2016) 1071–1078.
[32] M. Kitano, T. Kudo, M. Matsuoka, M. Ueshima, M. Anpo, Photocatalytic and photoelectrochemical properties of nitrogen-substituted TiO_2 thin films prepared by an RF magnetron sputtering deposition method, Mater. Sci. Forum 544–545 (2007) 107–110.
[33] U. Diebold, The surface science of titanium dioxide, Surf. Sci. Rep. 48 (2003) 53–229.
[34] S. Livraghi, M. Chiesa, M. Paganini, E. Giamello, On the nature of reduced states in titanium dioxide as monitored by electron paramagnetic resonance. I: the anatase case, J. Phys. Chem. C 115 (2011) 25413–25421.
[35] S. Livraghi, M. Rolando, S. Maurelli, M. Chiesa, M.C. Paganini, E. Giamello, Nature of reduced states in titanium dioxide as monitored by electron paramagnetic resonance. II: rutile and brookite cases, J. Phys. Chem. C 118 (2014) 22141–22148.
[36] E. Morra, E. Giamello, M. Chiesa, EPR approaches to heterogeneous catalysis. The chemistry of titanium in heterogeneous catalysts and photocatalysts, J. Magn. Reson. 280 (2017) 89–102.
[37] Z. Wang, W. Ma, C. Chen, H. Ji, J. Zhao, Probing paramagnetic species in titania-based heterogeneous photocatalysis by electron spin resonance (ESR) spectroscopy – a mini review, Chem. Eng. J. 170 (2011) 353–362.
[38] M. Fittipaldi, D. Gatteschi, P. Fornasiero, The power of EPR techniques in revealing active sites in heterogeneous photocatalysis: the case of anion doped TiO_2, Catal. Today 206 (2013) 2–11.
[39] A.E. Giannakas, E. Seristatidou, Y. Deligiannakis, I. Konstantinou, Photocatalytic activity of N-doped and N-F co-doped TiO_2 and reduction of chromium(VI) in aqueous solution: an EPR study, Appl. Catal. B 132–133 (2013) 460–468.
[40] A.M. Czoska, S. Livraghi, M.C. Paganini, E. Giamello, C. Di Valentin, G. Pacchioni, The nitrogen-boron paramagnetic center in visible light sensitized N-B co-doped TiO_2. Experimental and theoretical characterization, Phys. Chem. Chem. Phys. 13 (2011) 136–143.
[41] A.M. Czoska, S. Livraghi, M. Chiesa, E. Giamello, S. Agnoli, G. Granozzi, E. Finazzi, C. Di Valentin, G. Pacchioni, The nature of defects in fluorine-doped TiO_2, J. Phys. Chem. C 112 (2008) 8951–8956.
[42] Z. Barbieriková, D. Dvoranová, M.V. Sofianou, C. Trapalis, V. Brezová, UV-induced reactions of Mg^{2+}-doped anatase nanocrystals with exposed {001} facets: an EPR study, J. Catal. 331 (2015) 39–48.
[43] S. Livraghi, M.R. Chierotti, E. Giamello, G. Magnacca, M.C. Paganini, G. Cappelletti, C.L. Bianchi, Nitrogen-doped titanium dioxide active in photocatalytic reactions with visible light: a multi-technique characterization of differently prepared materials, J. Phys. Chem. C 112 (2008) 17244–17252.
[44] K.A. Michalow, D. Logvinovich, A. Weidenkaff, M. Amberg, G. Fortunato, A. Heel, T. Graule, M. Rekas, Synthesis, characterization and electronic structure of nitrogen-doped TiO_2 nanopowder, Catal. Today 144 (2009) 7–12.
[45] S. Livraghi, M.C. Paganini, E. Giamello, A. Selloni, C. Di Valentin, G. Pacchioni, Origin of photoactivity of nitrogen-doped titanium dioxide under visible light, J. Am. Chem. Soc. 128 (2006) 15666–15671.
[46] C. Di Valentin, G. Pacchioni, A. Selloni, S. Livraghi, E. Giamello, Characterization of paramagnetic species in N-doped TiO_2 powders by EPR spectroscopy and DFT calculations, J. Phys. Chem. B 109 (2005) 11414–11419.
[47] S. Livraghi, M.C. Paganini, M. Chiesa, E. Giamello, Trapped molecular species in N-doped TiO_2, Res. Chem. Intermed. 33 (2007) 739–747.
[48] M.N. Grecu, D. Macovei, D. Ghica, C. Logofatu, S. Valsan, N.G. Apostol, G.A. Lungu, R.F. Negrea, R.R. Piticescu, Co environment and magnetic defects in anatase $Co_xTi_{1-x}O_2$ nanopowders, Appl. Phys. Lett. 102 (2013) Article number 161909.
[49] M.N. Grecu, S. Constantinescu, D. Tărăbăşanu-Mihăilă, D. Ghica, I. Bibicu, Spin dynamics in ^{57}Fe-doped TiO_2 anatase nanoparticles, Phys. Status Solidi B 248 (2011) 2927–2931.
[50] M. Batzill, E.H. Morales, U. Diebold, Influence of nitrogen doping on the defect formation and surface properties of TiO_2 rutile and anatase, Phys. Rev. Lett. 96 (2006) 026103.
[51] E.A. Konstantinova, A.I. Kokorin, K. Lips, S. Sakthivel, H. Kisch, EPR study of the illumination effect on properties of paramagnetic centers in nitrogen-doped TiO_2 active in visible light photocatalysis, Appl. Magn. Reson. 35 (2009) 421–427.
[52] Y. Nosaka, A.Y. Nosaka, Generation and detection of reactive oxygen species in photocatalysis, Chem. Rev. 117 (2017) 11302–11336.
[53] H. Fu, L. Zhang, S. Zhang, Y. Zhu, J. Zhao, Electron spin resonance spin-trapping detection of radical intermediates in N-doped TiO_2-assisted photodegradation of 4-chlorophenol, J. Phys. Chem. B 110 (2006) 3061–3065.
[54] G. Veréb, L. Manczinger, G. Bozsó, A. Sienkiewicz, L. Forró, K. Mogyorósi, K. Hernádi, A. Dombi, Comparison of the photocatalytic efficiencies of bare and doped rutile and anatase TiO_2 photocatalysts under visible light for phenol degradation and E. coli inactivation, Appl. Catal. B 129 (2013) 566–574.
[55] J. Schneider, M. Matsuoka, M. Takeuchi, J. Zhang, Y. Horiuchi, M. Anpo, D.W. Bahnemann, Understanding TiO_2 photocatalysis: mechanisms and materials, Chem. Rev. 114 (2014) 9919–9986.
[56] D. Dvoranová, Z. Barbieriková, V. Brezová, Radical intermediates in photoinduced reactions on TiO_2 (an EPR spin trapping study), Molecules 19 (2014) 17279–17304.
[57] H.H. Lo, N.O. Gopal, S.C. Sheu, S.C. Ke, Electron paramagnetic resonance investigation of charge transfer in TiO_2(B)/anatase and N-TiO_2(B)/anatase mixed-phase nanowires: the relative valence and conduction band edges in the two phases, J. Phys. Chem. C 118 (2014) 2877–2884.
[58] E.G. Panarelli, S. Livraghi, S. Maurelli, V. Polliotto, M. Chiesa, E. Giamello, Role of surface water molecules in stabilizing trapped hole centres in titanium dioxide (anatase) as monitored by electron paramagnetic resonance, J. Photochem. Photobiol. A 322–323 (2016) 27–34.
[59] M. Hayyan, M.A. Hashim, I.M. Alnashef, Superoxide ion: generation and chemical implications, Chem. Rev. 116 (2016) 3029–3085.
[60] H. Zhao, J. Joseph, H. Zhang, H. Karoui, B. Kalyanaraman, Synthesis and biochemical applications of a solid cyclic nitrone spin trap: a relatively superior trap for detecting superoxide anions and glutathiyl radicals, Free Radic. Biol. Med. 31 (2001) 599–606.
[61] V. Brezová, S. Gabčová, D. Dvoranová, A. Staško, Reactive oxygen species produced upon photoexcitation of sunscreens containing titanium dioxide (an EPR study), J. Photochem. Photobiol. B 79 (2005) 121–134.
[62] V. Brezová, D. Dvoranová, A. Staško, Characterization of titanium dioxide photoactivity following the formation of radicals by EPR spectroscopy, Res. Chem. Intermed. 33 (2007) 251–268.
[63] P.J. Collins, A.D.W. Dobson, J.A. Field, Reduction of the 2,2'-azinobis(3-ethylbenzthiazoline-6-sulfonate) cation radical by physiological organic acids in the absence and presence of manganese, Appl. Environ. Microbiol. 64 (1998) 2026–2031.